Key Points:
- 3-D effects on the thermal structure of the subduction zone are investigated
- The effects on slab surface temperature are moderate
- The effects on surface heat flow are insignificant

Along-arc variation in the 3-D thermal structure around the junction between the Japan and Kurile arcs

Manabu Morishige[1] and Peter E. van Keken[2]

[1]Department of Deep Earth Structure and Dynamics Research, Japan Agency for Marine-Earth Science and Technology, Yokosuka, Japan, [2]Department of Earth and Environmental Sciences, University of Michigan, Ann Arbor, Michigan, USA

Abstract The thermal structure in subduction zones has a strong influence on seismogenesis and arc volcanism. Traditional 2-D models have been used to provide reasonable agreement between models and observations, but in a number of cases clear 3-D effects are present. One such case is in the Northern Japan subduction system. At the junction between Japan and Kurile arcs, surface heat flow and the occurrence of intermediate-depth seismicity are different than in the Tohoku and Hokkaido regions. We investigate the effects of 3-D slab geometry and a local deepening of slab-mantle decoupling depth on the thermal structure in this region based on 3-D finite element approach. We find that both effects produce the along-arc variation of slab surface temperature, which could reach ∼100°C. The warmer region arises through 3-D effects of thermal conduction and the colder region arises through localized slow incoming flow in the case where 3-D slab geometry is taken into account. 3-D flow arises where a local deepening of slab-mantle decoupling depth is assumed, which leads to both warmer and colder regions. The effects on surface heat flow are small. While intermediate-depth seismicity in the subducted crust is suggested to be controlled by temperature-dependent phase transitions, the predicted changes in thermal structure are not sufficient to cause the observed deepening of seismicity. This suggests that the thermal structure of this subduction zone may be more strongly influenced by time-dependent deformation of the overriding crust and slab.

1. Introduction

Our understanding about the thermal structure of the subduction zone has improved in the last few decades. The main factors controlling the thermal structure of the subduction zone are the heat advection due to cold subducting slab and hot flowing mantle. Thermal conduction also plays an important role near the slab surface and in the overriding plate.

Of particular importance is the cornerflow which arises due to the coupling between downgoing slab and overriding mantle wedge. The rheology of the wedge itself critically influences the heat transport to the slab, and therefore, directly controls the slab surface temperatures. *van Keken et al.* [2002], *Kelemen et al.* [2003], and *Conder* [2005] demonstrated that introducing a realistic olivine rheology leads to the focus of the flow in the mantle wedge. As a result, the temperature increases in the mantle wedge and on the slab surface by a few hundred degrees compared to older isoviscous models. The high below-arc temperatures are confirmed by a detailed benchmark for subduction zone models suggesting the governing equations are solved with high accuracy [*van Keken et al.*, 2008]. The effect of radiogenic heat production is small and primarily affects the thermal structure in the overriding plate [*Hall*, 2012]. Constraints from geophysical observations, in particular those of heat flow and seismic tomography [*Tsumura et al.*, 2000; *Bostock et al.*, 2002; *Hyndman and Peacock*, 2003; *Schurr et al.*, 2003; *Tanaka et al.*, 2004; *Eberhart-Phillips et al.*, 2008; *Rondenay et al.*, 2008], provide an indication that the mantle wedge in the fore arc is anomalously cold and apparently not involved in the cornerflow that is induced by the subducting slab. We can assume that over geological timescales the slab is effectively decoupled from the overlying plate due to frequent underthrusting earthquakes along the seismogenic zone that generally ends near 50 km depth. The observed cold corner requires that the slab is decoupled to greater depth by creeping or other aseismic but local deformation. In northern Japan, as well as in other well-instrumented subduction zones, the geometry of the cold corner is best explained when the slab couples to the overlying mantle wedge at depth of approximately 80 km [*Wada and Wang*, 2009].
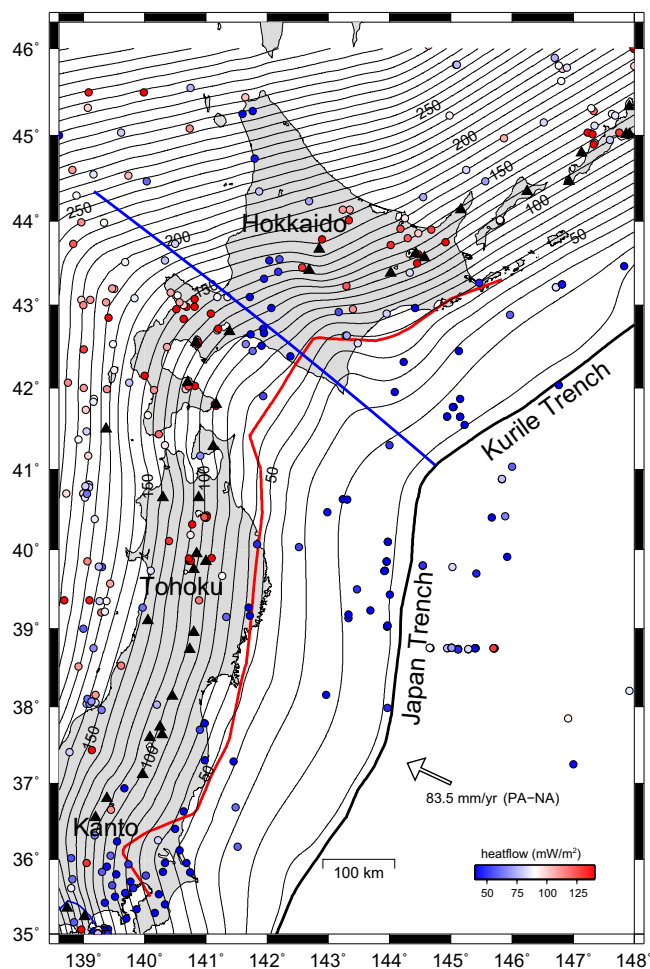
Figure 1. Summary of observations near the junction between Japan and Kurile arcs based on Figure 1 of *van Keken et al.* [2012]. Thick black line shows the location of Japan and Kurile trench. Thin black lines are the contours of slab surface every 10 km [*Zhao et al.*, 1997; *Nakajima and Hasegawa*, 2006; *Kita et al.*, 2010]. Colored circles show surface heat flow [*Tanaka et al.*, 2004]. Red line shows the downdip limit of low-angle thrust events [*Kita et al.*, 2010]. Blue line shows the location where we show the cross section in Figure 8b. Arrow shows relative movement of Pacific plate (PA) to North America plate (NA).

Honda [1985] first proposed using numerical model that the rigid fore-arc mantle is necessary to explain the low surface heat flow region in the northeast Japan. *Wada and Wang* [2009] extended the work to a wide range of subduction zones and proposed the idea of common depth of slab-mantle decoupling. The slab-mantle decoupling depth is a depth such that the mantle does not move with the slab above it and the mantle moves with the same velocity as the slab beneath it. The transition in the rheology and resulting nonlinear feedback between thermal structure and flow geometry causes the near-stagnation of the shallow wedge with resulting lower temperatures [*Kneller et al.*, 2007; *Wada et al.*, 2011].

The use of thermal modeling is particularly useful in direct comparisons with the temperature estimates from arc geochemistry and petrology. In recent years, we have seen good agreement between model predictions and geochemical observations. Application of the H_2O-Ce thermometer to determine slab fluid temperatures has shown good correspondence with a specific thermal model for Kamchatka [*Plank et al.*, 2009]. Application of the same technique to 10 subduction zones [*Cooper et al.*, 2012] also show remarkable agreement between geochemical estimates of the slab surface temperature to those predicted in a global study using two-dimensional finite element models [*Syracuse et al.*, 2010].

The models from *Syracuse et al.* [2010] also compare favorably with trace and major element mixing models for the Chilean [*Jacques et al.*, 2013; *Watt et al.*, 2013] and the Philippine arcs [*Turner et al.*, 2011]. Since geochemical and petrological analyses can be diagnostic for temperature variations that are significantly smaller than 100°C it is critical for us to develop an understanding of how 3-D variations in subduction geometry and flow can influence slab and wedge temperatures.

In this study, we consider the region around the junction between Japan and Kurile arcs (Figure 1). The subduction occurs nearly normal to the trench beneath Japan arc (Tohoku region), whereas an oblique subduction occurs beneath Kurile arc (Hokkaido region). Numerous studies on the Tohoku thermal structure have been made with 2-D modeling [e.g., *Honda*, 1985; *Peacock and Wang*, 1999; *van Keken et al.*, 2002, 2012], which appears appropriate due to limited along-arc variations. There are only a few studies focusing on an oblique subduction with 3-D models which is appropriate for the transition into Hokkaido [e.g., *Honda and Yoshida*, 2005; *Kneller and van Keken*, 2008; *Bengtson and van Keken*, 2012]. The number of numerical studies which consider these two regions together is quite small [*Morishige et al.*, 2010; *Morishige and Honda*, 2013]. *Morishige and Honda* [2013] showed that the along-arc variation of seismic anisotropy [e.g., *Nakajima et al.*,

2006], subduction angle [e.g., *Hayes et al.*, 2012], and the slab behavior in the transition zone [e.g., *Fukao et al.*, 2001; *Miller and Kennett*, 2006] can be explained at least qualitatively by the effects of the trench shape.

In this study, we focus on two other types of observations in this region which are affected by the thermal structure of the subduction zone.

The surface heat flow observations for northern Japan [*Tanaka et al.*, 2004] show the sharp transition from low values in the fore arc to high and scattered values in the arc and back arc. In southern Hokkaido, an anomalous incursion of low heat flow values occurs toward the Japan Sea (Figure 1). This suggests that the crust and mantle beneath this region is anomalously cold. *Kita et al.* [2010, 2012] imaged an anomalously low seismic velocity area below this region and proposed the presence of subducted continental crust. It may be caused by the southwestward migration of Kurile fore-arc sliver due to oblique subduction of Pacific plate since the middle Miocene [*Kimura*, 1986]. The presence of this block was also suggested to cause the anomalous deepening of the seismic belt in this region [*Kita et al.*, 2010] although a subsequent study that took this lower crustal root into account could not conclusively link the shift in seismicity to the modified thermal structure [*van Keken et al.*, 2012].

The upper plane of intermediate-depth seismicity below southern Hokkaido is different from its surroundings. While the seismicity of the upper plane remains in the crust, it occurs deeper than in the surrounding regions to the north and south [*Kita et al.*, 2010] and it gets closer to the slab surface in deeper part, whereas the seismicity diverges from slab surface with depth in other regions [*van Keken et al.*, 2012]. It suggests a modified dynamic or thermal regime there [*Kita et al.*, 2010]. *van Keken et al.* [2012] showed with a series of 2-D numerical models that the location of the blueschist-eclogite transition in the subducted oceanic crust overlaps with the termination of crustal seismicity in Tohoku and Hokkaido, but not beneath the junction between them.

We note that an anomalous area with deepened seismicity and an extended low surface heat flow region occurs also beneath Kanto [*Tanaka et al.*, 2004; *Hasegawa et al.*, 2007], but this is beyond the scope of this study.

In this study, we will test whether the anomalous heat flow and intermediate-depth seismicity are caused simply by 3-D effects near this junction, as was proposed in *van Keken et al.* [2012]. Toward this goal, we consider three types of cases. The first case focuses on the effects only of 3-D slab geometry. In the second case, we take into account the possible deepening of the transition from underthrusting and slow slip events to full coupling along the plate interface. The downdip limit of low angle thrust earthquakes beneath the junction is deeper than its surroundings by around 15 km (red line in Figure 1), which may be possibly due to subducted fore-arc crust [*Kita et al.*, 2010]. In the third case, we consider the two types of effects mentioned above together.

2. Modeling Approach

We divide the model domains into three parts: the crust, the mantle wedge, and the subducting slab. The x-z cross section is the same along the strike of the trench (y-direction) in all the cases considered except for the slab-mantle decoupling depth as we will show later (Figure 2a). The crust thickness is 25 km and the subduction angle is 30°. We consider three cases where slab geometry and/or the slab-mantle decoupling depth differ (Figure 2c).

In Case 1, we use the slab geometry similar to that of the junction between Japan and Kurile arcs to see the effects of 3-D slab geometry on the thermal structure. Slab-mantle decoupling depth (D_{dec}) is constant along the strike of the trench and set to be 80 km [*Wada and Wang*, 2009].

In Case 2, we use a simple slab geometry but include a local deepening of slab-mantle decoupling depth which is constrained from the along-arc variation of downdip limit of low angle thrust earthquakes [*Kita et al.*, 2010]. It is given as D_{dec} [km]$=87.5+7.5\sin((y-175)\pi/50)$ (at y [km] $\geq$ 150) and 80 (at y [km] < 150), which means that D_{dec} ranges from 80 to 95 km.

In Case 3, we use the same slab geometry as that used in Case 1, but the slab-mantle decoupling depth is given as D_{dec} [km]$=87.5+7.5\sin((y-275)\pi/50)$ (at 250 km $\leq$ y $\leq$ 350 km) and is kept constant at 80 km elsewhere.
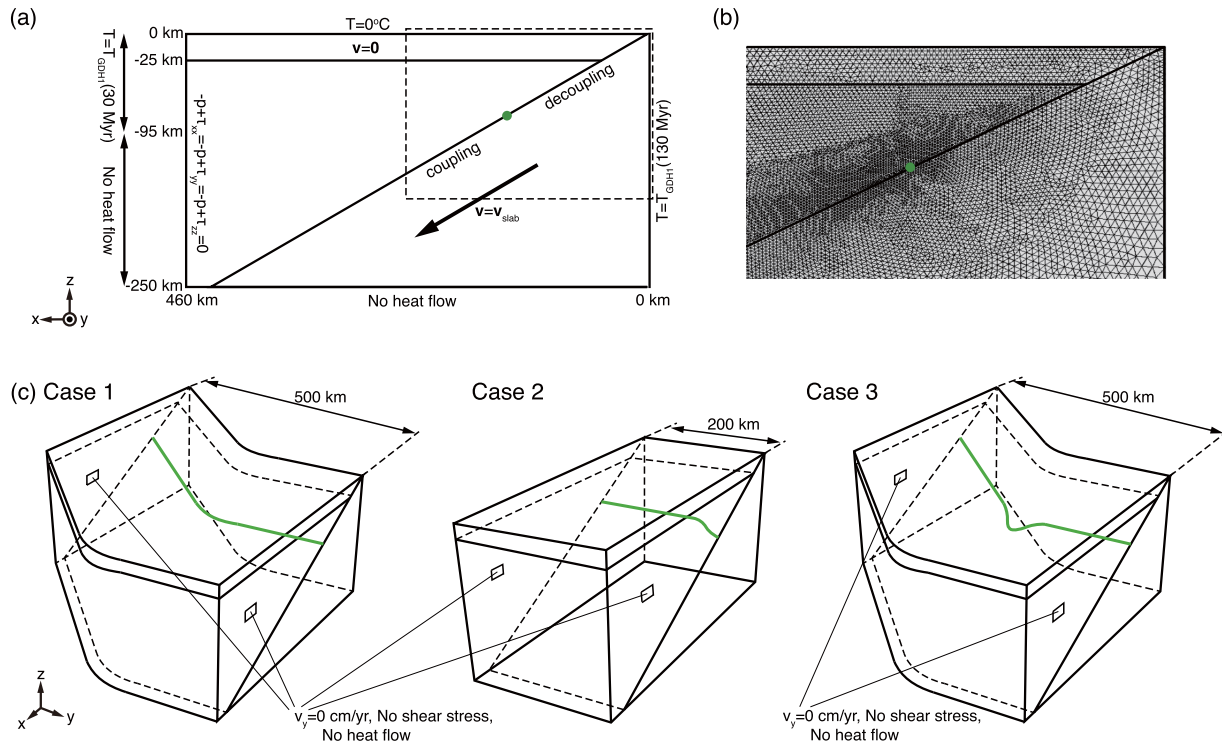
Figure 2. Numerical models. (a) Model geometry and boundary conditions in x-z cross section. (b) An example of mesh in the region enclosed by a dashed line in Figure 2a. (c) Model geometries and boundary conditions in 3-D view. The green points in Figures 2a and 2b, and the green lines in Figure 2c show the location of slab-mantle decoupling depth.

The mantle flow is computed only in the mantle wedge by solving the equations of mass conservation and motion for an incompressible infinite Prandtl number fluid without buoyancy forces:

$$\nabla \cdot \underline{v} = 0, \tag{1}$$

$$\nabla \cdot \underline{\underline{\tau}} - \nabla p = 0, \tag{2}$$

$$\underline{\underline{\tau}} = 2\eta\underline{\dot{\epsilon}}, \tag{3}$$

where $\underline{v}$ is velocity, $\underline{\underline{\tau}}$ is the deviatoric stress tensor, p is dynamic pressure, η is effective viscosity, and $\underline{\dot{\epsilon}}$ is strain rate tensor defined by

$$\underline{\dot{\epsilon}} = \frac{1}{2}\left(\left(\nabla\underline{v}\right) + \left(\nabla\underline{v}\right)^{\mathrm{T}}\right). \tag{4}$$

We assume a rigid boundary $\underline{v} = \underline{0}$ between the mantle wedge and the crust. The velocity boundary condition at the slab surface depends on the depth considered. Below the slab-mantle decoupling depth, we impose $\underline{v} = \underline{v}_{\mathrm{slab}} = (V_0\cos 30^{\mathrm{o}}, \quad 0, \quad -V_0\sin 30^{\mathrm{o}})$ with $V_0 = 8$ cm/yr while above this depth the velocity boundary condition is zero. $\underline{v}$ changes from $\underline{0}$ to $\underline{v}_{\mathrm{slab}}$ linearly over 6 km along the slab surface around the slab-mantle decoupling depth to mitigate the effects of the pressure singularity that arises with a discontinuous velocity boundary condition as discussed in *van Keken et al.* [2002]. The wedge inflow/outflow boundaries are assumed to be $-p+\tau_{xx} = -p+\tau_{yy} = -p+\tau_{zz} = 0$ leading to free inflow and outflow. We assume $v_y = 0$ cm/yr and zero shear stress at the boundaries in y-direction.

We solve the time-dependent heat equation for the whole domain. We ignore radiogenic heat production and assume the Boussinesq approximation:

$$\frac{\partial T}{\partial t} + \underline{v} \cdot \nabla T = \kappa\nabla^2 T, \tag{5}$$

where T is temperature, t is time, and κ ($=7.272 \times 10^{-7}$ m^2/s) is thermal diffusivity. In solving this equation, the velocity in the crust and subducting slab are assumed to be $\underline{0}$ and $\underline{v}_{slab}$, respectively. The surface boundary condition is 0°C and the GDH1 model [*Stein and Stein*, 1992] is used to define the temperature at the wedge inflow (assuming an age of 30 Myr appropriate for the Japan Sea) and slab inflow (with an age of 130 Myr). GDH1 model is a plate cooling model where the plate thickness is 95 km and the potential temperature at the bottom of the plate is 1421.5°C. No heat flow is assumed at other boundaries. We assume the constant adiabatic temperature gradient of 0.3 K/km that we add as a postprocessing step.

We consider dislocation creep in the mantle wedge. The effective viscosity for this deformation mechanism can be written as

$$\eta_{disl}(T, \dot{\epsilon}) = A_{disl} \exp\left(\frac{E_{disl}}{nRT}\right) \dot{\epsilon}^{(1-n)/n}, \tag{6}$$

where $A_{disl} = 2.8968 \times 10^4$ Pa · s$^{1/n}$ is constant, $E_{disl} = 540$ kJ/mol is activation energy, $R = 8.3145$ J/K/mol is the gas constant, $n = 3.5$ is a constant, and $\dot{\epsilon}$ is the second invariant of strain rate tensor defined as

$$\dot{\epsilon} = \sqrt{\frac{1}{2} \dot{\epsilon}_{ij} \dot{\epsilon}_{ij}}. \tag{7}$$

The values of these parameters are based on *Karato and Wu* [1993] for dry olivine.

The effective viscosity used in equation (3) is defined by

$$\eta = \left(\frac{1}{\eta_{disl}} + \frac{1}{\eta_{max}}\right)^{-1}, \tag{8}$$

where $\eta_{max} = 10^{24}$ Pa · s is the maximum viscosity.

We use the finite element code Sepran [*Cuvelier et al.*, 1986] with a linear tetrahedral mesh to solve these equations. The minimum linear element size is 1.5 km around the slab-mantle decoupling depth (Figure 2b) with the resolution of elements increasing to 20 km in areas of small temperature variations. We conducted convergence tests for an essentially 2-D case (3-D case with no along-arc variation) and found that this resolution is acceptable. We use GDH1 model [*Stein and Stein*, 1992] with an age of 30 Myr as the initial thermal structure. We evolve the time-dependent models for 20 Myr and use a time step of 0.38 Myr.

3. Results

In this section, we mainly focus on the slab surface temperature and surface heat flow in each of the three cases. The surface heat flow is defined by

$$F = -k \frac{dT}{dz}, \tag{9}$$

where $k = 3$ W/m/K is the thermal conductivity.

3.1. Case 1: Effects of 3-D Slab Geometry

Figure 3 shows the results of the case focusing on the effects of 3-D slab geometry on the thermal structure of the subduction zone. The curvature radius R_C of the junction is ~141.4 km in this case.

We can see first that the slab surface temperature is slightly higher where an oblique subduction occurs compared to where the subduction occurs normal to the trench (compare, for example, the temperature at y = 150 km and y = 500 km, Figure 3a). Near the junction, we can see a colder region at y ~ 360 km and a warmer region at y ~ 255 km on the slab surface. The minor departures near y = 0 km are caused by the assumed flow boundary condition there and can be ignored.

Surface heat flow shows the general trend that it is low near the trench and high far from the trench, but there is no significant along-arc variation (Figure 3b). Horizontal velocity of the mantle flow shows that the
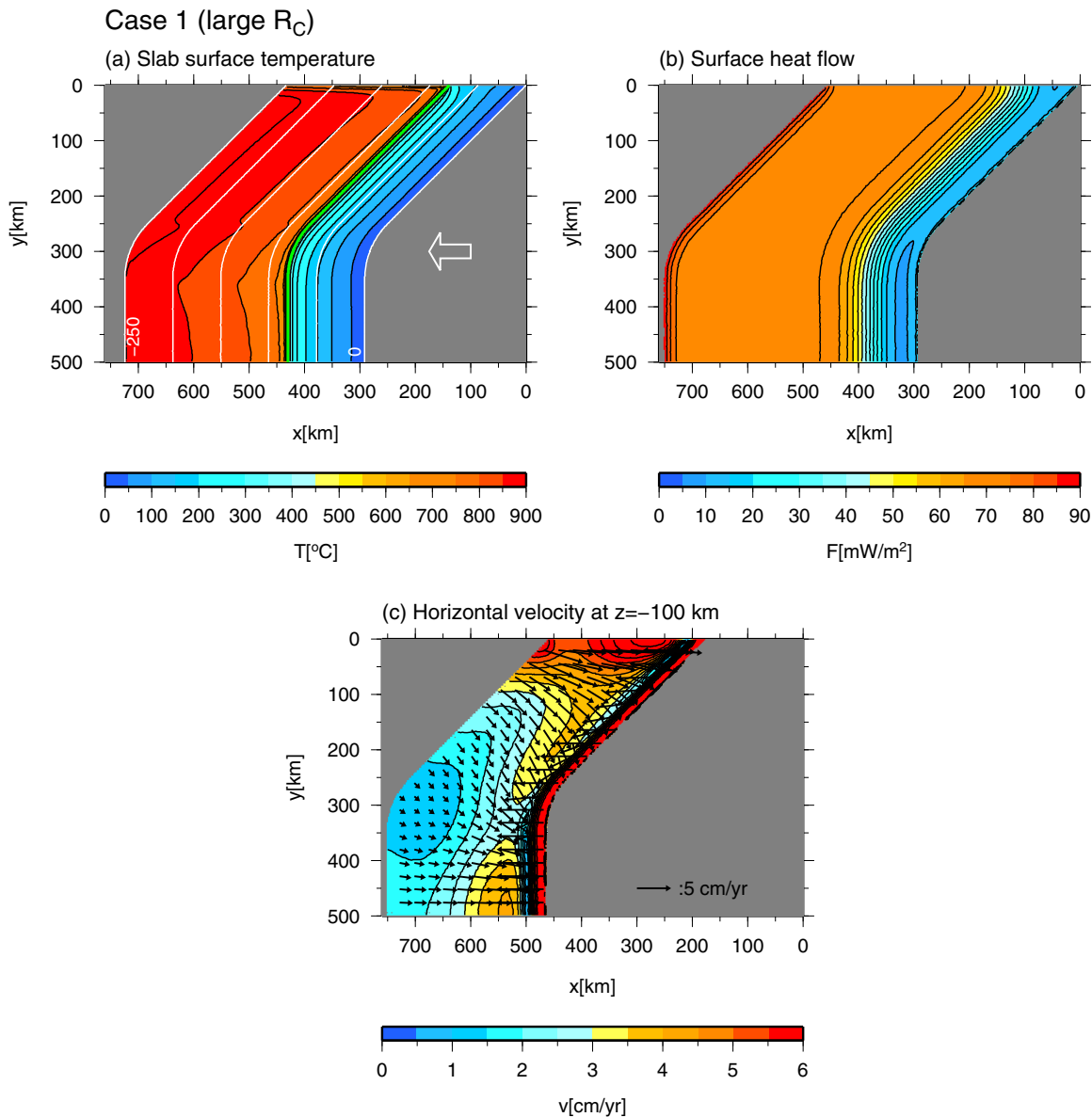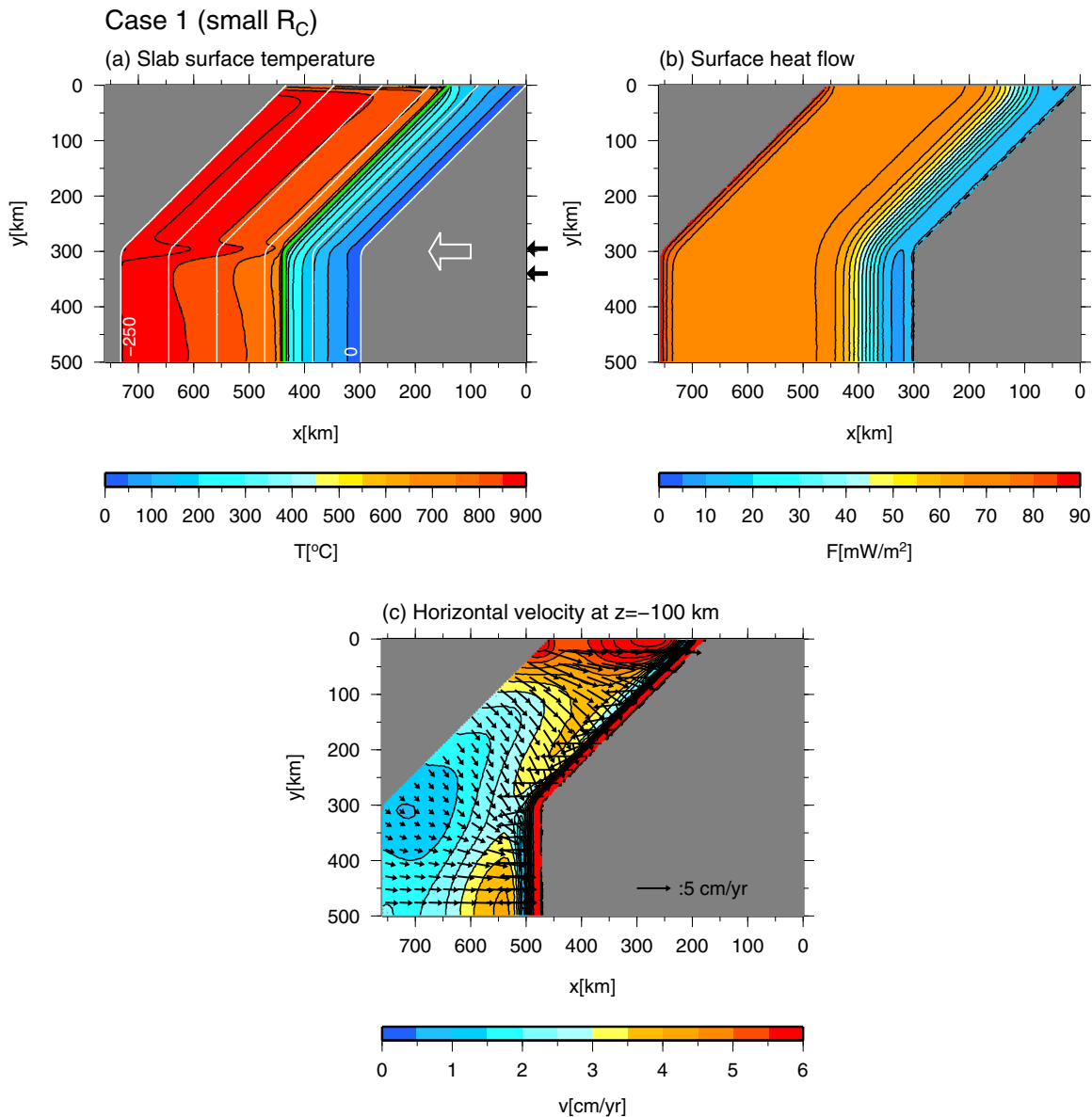
Figure 3. Results of Case 1 with a large curvature radius (R_C). (a) Slab surface temperature. Color shows temperature and white lines show the contours of slab surface every 50 km depth. Arrow shows the direction of plate motion. Green line shows assumed slab-mantle decoupling depth. (b) Surface heat flow. (c) Horizontal velocity at 100 km depth. Arrows show horizontal velocity and color shows its magnitude $\sqrt{v_x^2 + v_y^2}$.

direction of incoming flow is nearly normal to the trench, but a region where the flow velocity is low arises near the junction (at $y \sim 350$ km, Figure 3c).

We also investigate the effects of the smoothness of the junction (Figure 4). In this case, the curvature radius R_C of the junction is smaller (~ 28.3 km). The colder region on the slab surface at $y \sim 340$ km is similar to the case with a larger curvature radius, but we can see the warmer region more clearly at $y \sim 295$ km in this case (Figure 4a). The surface heat flow and horizontal velocity of the mantle flow are similar to the case with a larger curvature radius (Figures 4b and 4c).

3.2. Case 2: Effects of a Local Deepening of Slab-Mantle Decoupling Depth

We show the results of the case focusing on the effects of a local deepening of slab-mantle decoupling depth (Figure 5). The increase of slab surface temperature at the slab-mantle decoupling depth is larger where we assume a local deepening of slab-mantle decoupling depth, which produces a warmer region

Figure 4. (a–c) Results of Case 1 with a small curvature radius (R_C) (same as in Figure 3). The arrows on the right side of Figure 4a show the position of the warmer and colder regions where we consider the cross sections in Figure 8.

there (at y ∼ 200 km, Figure 5a). There is a region with a slightly lower temperature just next to it at y ∼ 160 km. The along-arc variation of surface heat flow is insignificant (Figure 5b). The mantle flow in the wedge shows a significant 3-D pattern in the region where a local deepening of the slab-mantle decoupling depth is assumed (Figure 5c). The mantle flow spreads in the direction parallel to the trench (y-direction) near the slab-mantle decoupling depth at y ∼ 200 km. The material first located near the top moves in y-direction over a long distance (path 3), whereas the material first located far from the top does not move significantly in the y-direction (paths 1 and 2). The material where the slab-mantle decoupling depth is constant shows a more common 2-D cornerflow pattern (paths 4 and 5).

3.3. Case 3: Combination of Case 1 and Case 2

Figure 6 shows the results of the case where we consider the combined effects of 3-D slab geometry and a local deepening of slab-mantle decoupling depth. We observe two warmer regions at y ∼ 255 km, 300 km and a colder region at y ∼ 355 km (Figure 6a). There again is little change in surface heat flow along the
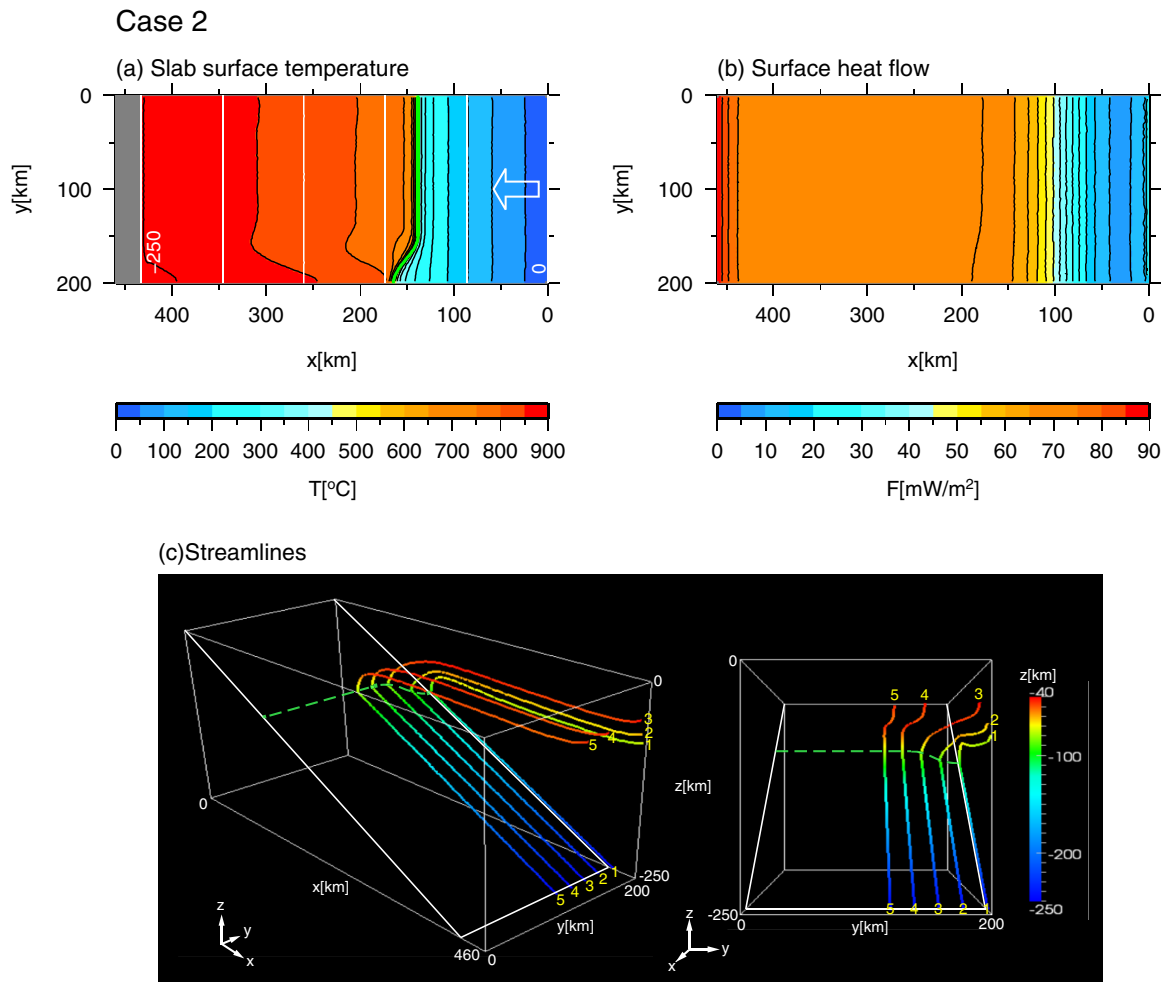
Case 2

Figure 5. (a, b) Results of Case 2 (as in Figure 3). (c) 3-D views of streamlines with a numbering. The green dashed line shows assumed slab-mantle decoupling depth. The color of streamlines shows z-coordinate along each streamline.

strike of the trench (Figure 6b). Horizontal velocity of the mantle flow is similar to that in Case 1 with a large curvature radius of the junction (Figure 3c), although we can see a slight difference near the junction (at y ∼ 350 km, Figure 6c).

3.4. Steady State Cases

The three cases discussed above are based on a 20 Myr evolution of the time-dependent model. This is sufficient to bring the slab thermal structure of 2-D models into a quasi steady state. A longer evolution will cause changes in the thermal structure of the overriding plate, which is relevant for surface heat flow. *Hall* [2012] discussed the difference between the results in steady state and time-dependent cases using simple 2-D subduction zone models, similar to *van Keken et al.* [2008]. We evaluate how the assumption of pure steady state, where we do not solve the time-dependent equations but assume $\partial T/\partial t = 0$ in equation (5), affects the thermal structure in these 3-D models.

Figures 7a and 7b are the results obtained assuming steady state for Case 1 with a large curvature radius of the junction. Intriguingly, the slab surface temperature clearly differs from that in time-dependent case for Case 1. Specifically, the colder region (at y ∼ 390 km) is more pronounced (cf. Figures 3a and 7a).

On the other hand, the difference in slab surface temperature between steady state and time-dependent cases for Case 2 is rather small (cf. Figures 5a and 7c).

The surface heat flow shows slightly more distinct along-arc variation in the steady state cases (Figures 7b and 7d). The thermal structure of the overriding plate is somewhat more affected by the underlying thermal
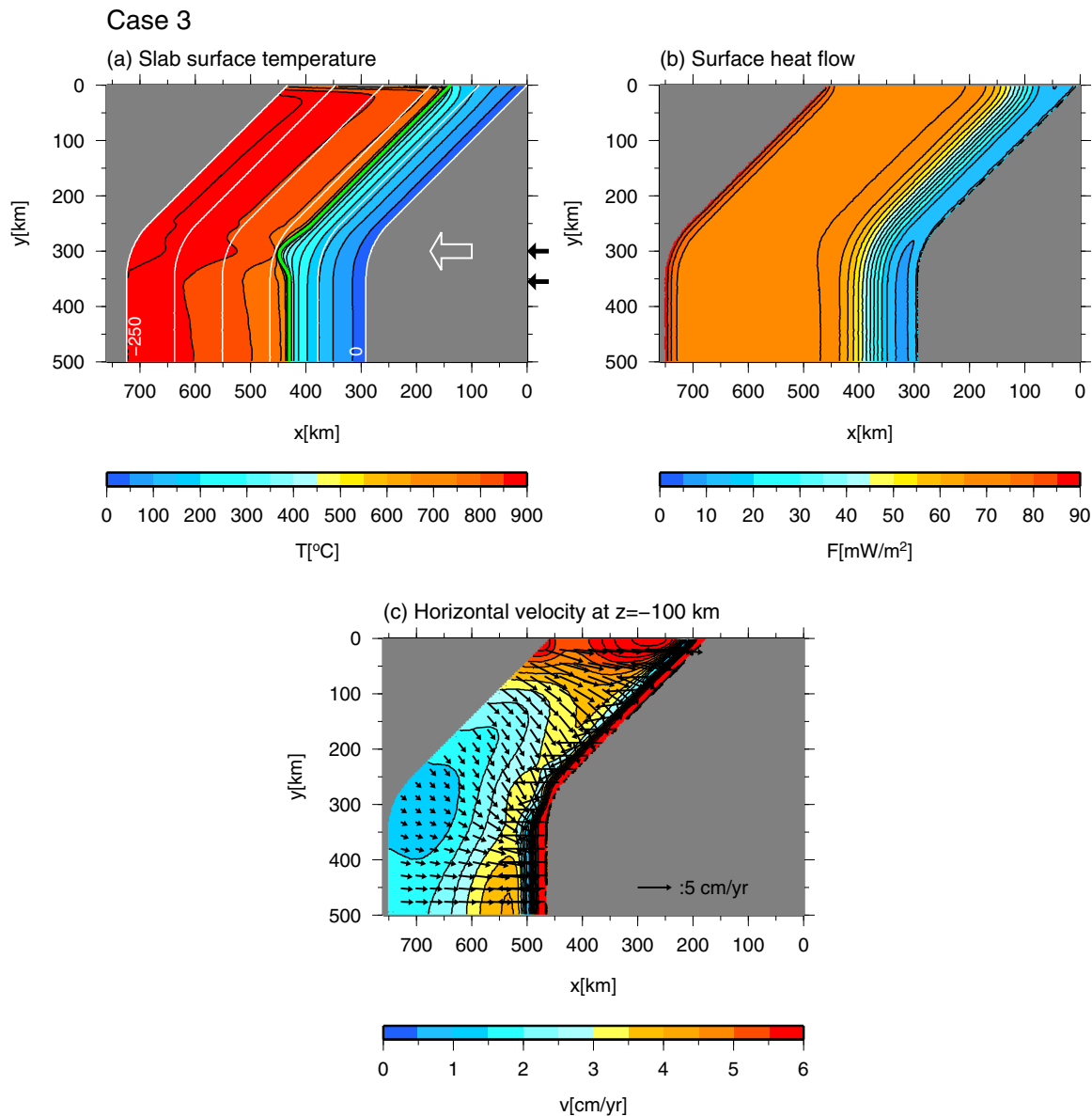
Figure 6. Results of Case 3 with descriptions as in Figure 4.

structure. The along-arc variation of surface heat flow in Case 2 directly reflects the assumed slab-mantle decoupling depth. Note that the values of surface heat flow are lower in steady state cases as a whole, which is caused by the conductive thickening of lithosphere of the overriding plate.

4. Discussion

4.1. Slab Surface Temperature

We showed that the along-arc variation of slab surface temperature arises by the effects of 3-D slab geometry and a local deepening of slab-mantle decoupling depth. In this subsection, we consider the possible causes of these thermal anomalies. First, we saw that slab surface temperature is generally higher where an oblique subduction occurs compared to where the subduction occurs normal to the trench. It can be explained by the effects of subduction obliquity. *Bengtson and van Keken* [2012] showed that the slab surface temperature in an oblique subduction case was identical to that obtained in a 2-D cross section which is taken normal to the trench. We consider a proxy of the temperature in the slab called thermal parameter Φ [*Kirby et al.*, 1991] (which is defined as $\Phi = Av_p \sin\theta$ where A is plate age, v_p is slab speed, and θ is
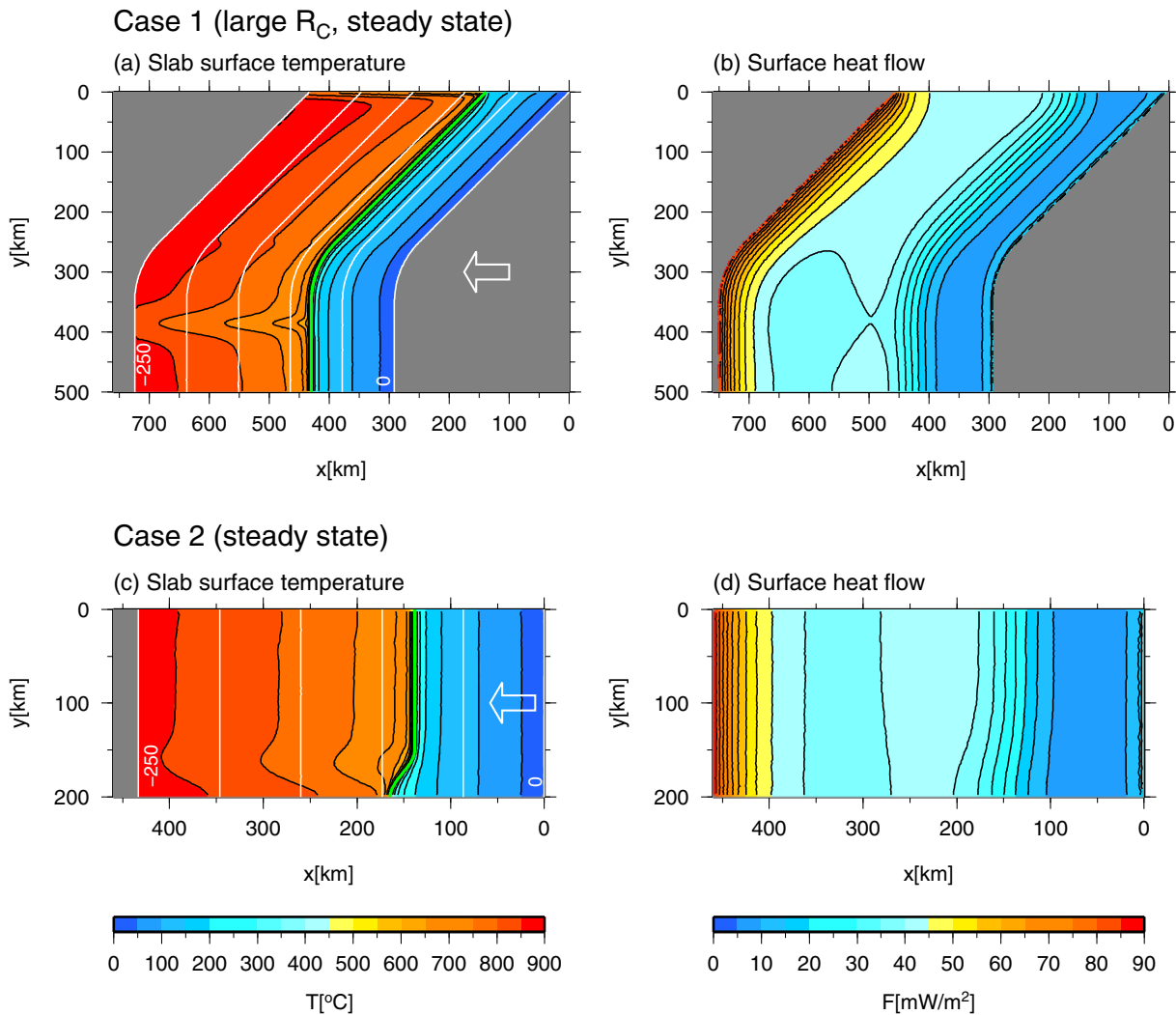
Figure 7. Steady state results. (a, b) Results of Case 1 with a large curvature radius, (c, d) Case 2 where steady state is assumed. Figures 7a and 7c are the same as Figure 3a, and Figures 7b and 7d are the same as Figure 3b.

subduction angle which are taken in the trench-normal direction). In the cross section normal to the trench $\Phi=4648$ km where an oblique subduction occurs (note that the maximum angle between the direction of subduction and the strike of the trench is 45°), but it increases to 5200 km where the subduction occurs normal to the trench. This increase explains the difference of slab surface temperature in the two regions. In Case 1, a region with slower incoming flow (Figures 3c and 4c) also causes less rapid warming of the slab surface near the junction, as is indicated by the overlap in location of slow flow and low slab surface temperature (at y ∼ 350 km). Changes in the curvature radius of the junction (R_C) are less important (Figures 3c and 4c), demonstrating that the large-scale flow in the mantle wedge is not affected by the smoothness of the junction at least for the range of R_C considered in this study.

Interestingly, the warmer region seen in Cases 1 (at y ∼ 255 km in Case 1 with large curvature radius and y ∼ 295 km in Case 1 with low curvature radius) appear to be caused by thermal conduction as the slab is warmed from two different horizontal directions (from the left and upper left directions, Figures 3a and 4a), so the temperature rises. The fact that this effect is weaker when the junction is smoother supports this idea (Figures 3a and 4a).

In Case 2, we saw that a local deepening of slab-mantle decoupling depth leads to a 3-D flow in the mantle wedge (Figure 5c). The warmer region at y ∼ 200 km arises because the material here originally comes from relatively deeper and warmer part (paths 1 and 2). The warmer slab surface for a larger decoupling depth is
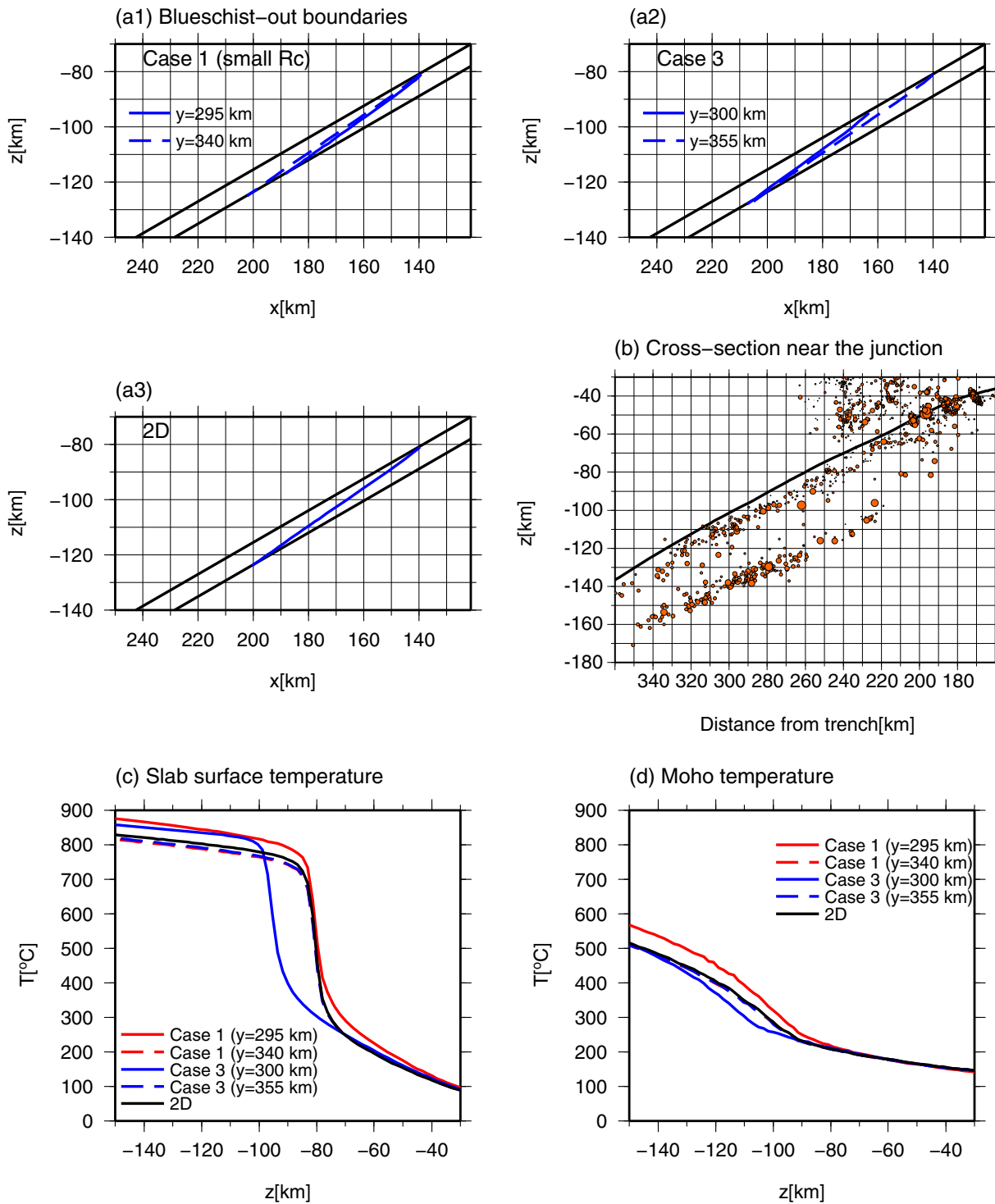
Figure 8. (a) Predicted blueschist-out boundaries at several cross sections for (a1) Case 1 with small curvature radius, (a2) Case 3, and (a3) 2-D case for comparison. Black lines show upper and lower boundaries of the oceanic crust. We assume that the width of the oceanic crust is 7 km. Blue lines show predicted blueschist-out boundaries. (b) Cross section near the junction based on P15 of Figure 6 in *van Keken et al.* [2012]. The line where the cross section is taken is shown in Figure 1 with blue line. Black line shows slab surface, orange circles are seismicity within 10 km from the cross section where their size shows magnitude. (c) Slab surface temperature. (d) Moho temperature.

also observed in 2-D models [*Wada et al.*, 2008]. The path 3 includes the motion in y-direction compared to paths 4 and 5, so it takes longer time for the material to move down to a certain depth on the slab surface along this path. It means that the material which moves along the path 3 is cooled for longer time, which leads to the colder region at y ∼ 160 km.

The slab surface temperature distribution in Case 3 may be understood simply by combining the results obtained in Cases 1 and 2. The effects of 3-D slab geometry may cause the warmer region at y ∼ 255 km and the colder region at y ∼ 355 km, as we have seen in Case 1. The warmer region at y ∼ 300 km is likely due to 3-D flow caused by a local deepening of slab-mantle decoupling depth as in Case 2.

4.2. Intermediate-Depth Seismicity

We now turn to the question whether the changes in slab temperature can explain the deepening of the seismic belt below southern Hokkaido as suggested by *van Keken et al.* [2012] based on observations by *Kita et al.* [2010]. Since in most of the Tohoku and Hokkaido subduction systems, the upper plane seismicity is restricted to the region where blueschist facies rocks are predicted and disappear where eclogite facies rock should occur [*van Keken et al.*, 2012], we calculate the blueschist-out boundaries for Case 1 (with low curvature radius) and Case 3 and compare these to a 2-D case (Figures 8a1–8a3). We assume that the blueschist-out boundary is described by T [°C] = 617 − 52 P [GPa] where P is pressure [*Hacker*, 2008]. The pressure is calculated by using the values 2700 and 3300 kg/m^3 as the density of crust and mantle materials, respectively. First, the result of 2-D case shows that blueschist-out boundary starts at 80 km depth and ends at 125 km depth. The depth it starts may be controlled mainly by assumed slab-mantle decoupling depth. The result of Case 1 shows that the depth they start are the same (i.e., at 80 km) for the cross sections in the cold and warm regions, but the depth where it ends is shallower for the warm region. It is because that the difference in slab surface temperature remains at Moho depth (red lines in Figures 8c and 8d). In Case 3, on the other hand, the depth at which the blueschist-out boundaries start differs for the cross sections in the cold and warm regions, which reflects the change in decoupling depth. However, this difference is recovered deeper in the subducting oceanic crust. It reflects the fact that the difference in Moho temperature becomes small at deeper part (blue lines in Figure 8d). This feature can be seen also in 2-D numerical models [*van Keken et al.*, 2012]. We also calculate blueschist-out boundaries in the cross sections far from the junction (at y = 150 and 500 km) for Cases 1 and 3, and find that the obtained blueschist-out boundaries start at around 80 km depth and diverge from slab surface with depth, which are broadly consistent with observed intermediate-depth seismicity below Tohoku and Hokkaido (results not shown).

At the junction between Japan and Kurile arcs, *van Keken et al.* [2012] showed that the intermediate-depth seismicity may occur a few kilometer beneath the slab surface in the shallow part and then gradually get closer to the slab surface with depth (Figure 8b). However, we do not observe this kind of trend at the junction in any of the cases considered in this study. Using a different rheology or a large value of maximum slab-mantle decoupling depth increases the variation of slab surface temperature but does not help explain the distribution of the seismicity (Appendix A).

This clearly suggests that the 3-D flow geometry modeled here, even with changes in decoupling depth, cannot satisfactorily explain the deepening and relative location to slab surface of the seismic belt. One suggestion is that 3-D deformation of the slab (which is ignored here) can be important in causing the changes in thermal structure and modification of the blueschist-eclogite facies transition.

A second suggestion is that the relative location of the intermediate-depth seismicity in relation to the slab surface is not as precise beneath the junction as it is further south in Tohoku, since they are not determined simultaneously there [*Kita et al.*, 2010], although we observe that the correlation between seismicity and predicted mineral facies is recovered also in Hokkaido north of the junction [*van Keken et al.*, 2012].

An alternative suggestion for the deepening of the seismic belt could also be a kinetic delay of the phase change, although this begs the question why the kinetic conditions would be different in the junction but not elsewhere in the Northern Japan subduction zones.

4.3. Surface Heat Flow

In the cases considered in this study, we see only very minor along-arc variation in surface heat flow (Figures 3b, 4b, 5b, and 6b). The variations are slightly larger in the steady state cases (Figures 7b and 7d), but still much weaker than the clear heat flow excursion that is observed [*Tanaka et al.*, 2004] (Figure 1).
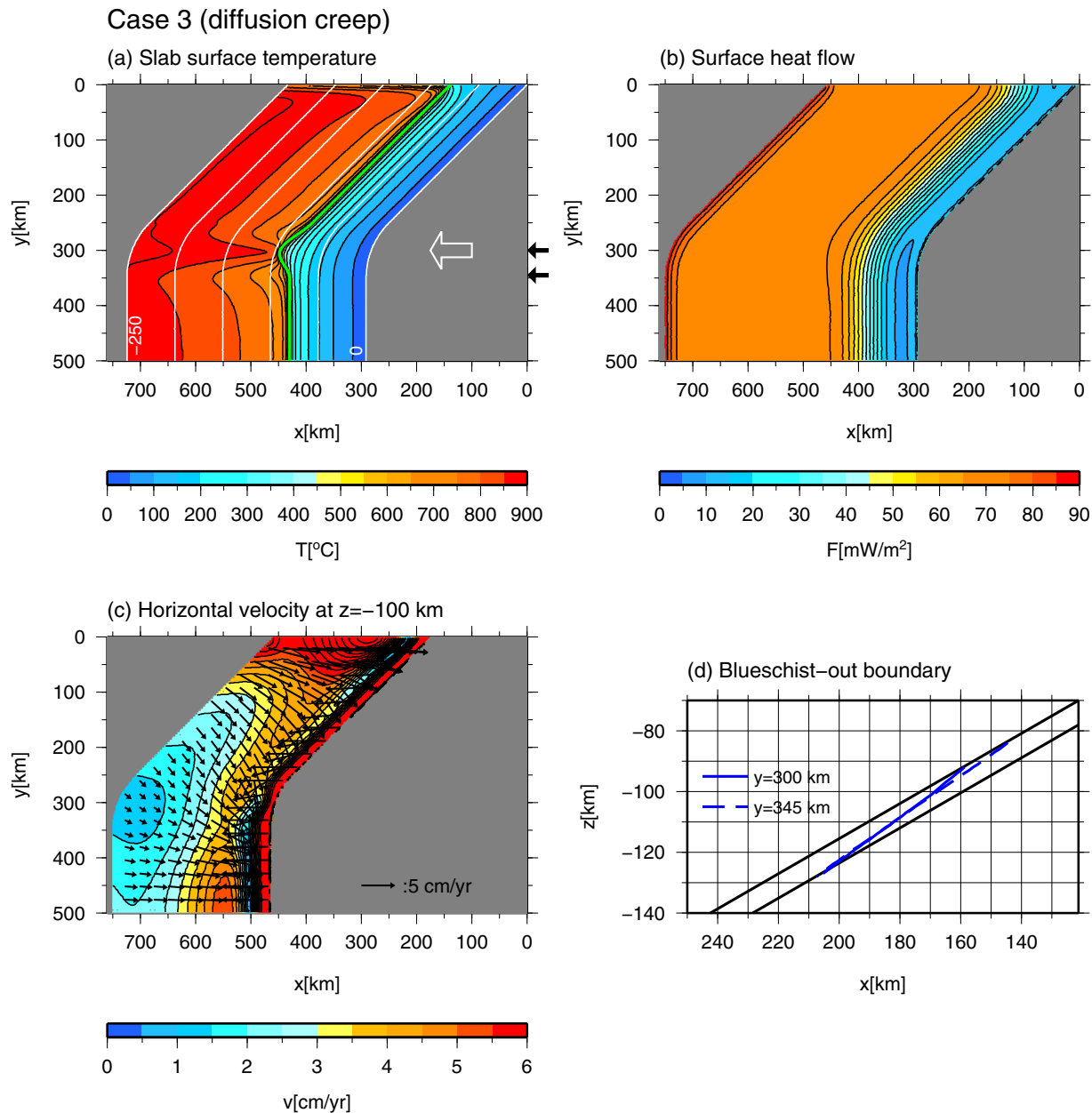
Figure A1. Results of Case 3 with diffusion creep instead of dislocation creep. Figures A1a–A1c as in Figures 6a–6c. Figure A1d as in Figure 8a.

For now, the best candidate to explain the low surface heat flow region at the junction may be the possible existence of subducted fore-arc crust [e.g., *Kita et al.*, 2010, 2012].

We plan on future studies that will include the time-dependent behavior of fore-arc crust, a realistic Moho structure [*Katsumata*, 2010] and the associated changes in radiogenic heat production, to develop a better understanding of surface heat flow in this region.

5. Conclusion

We investigated the effects of 3-D slab geometry and a local deepening of slab-mantle decoupling depth on thermal structure of the subduction zone near the junction between Japan and Kurile arcs. We found that both effects produced the along-arc variation of slab surface temperature which includes regions that
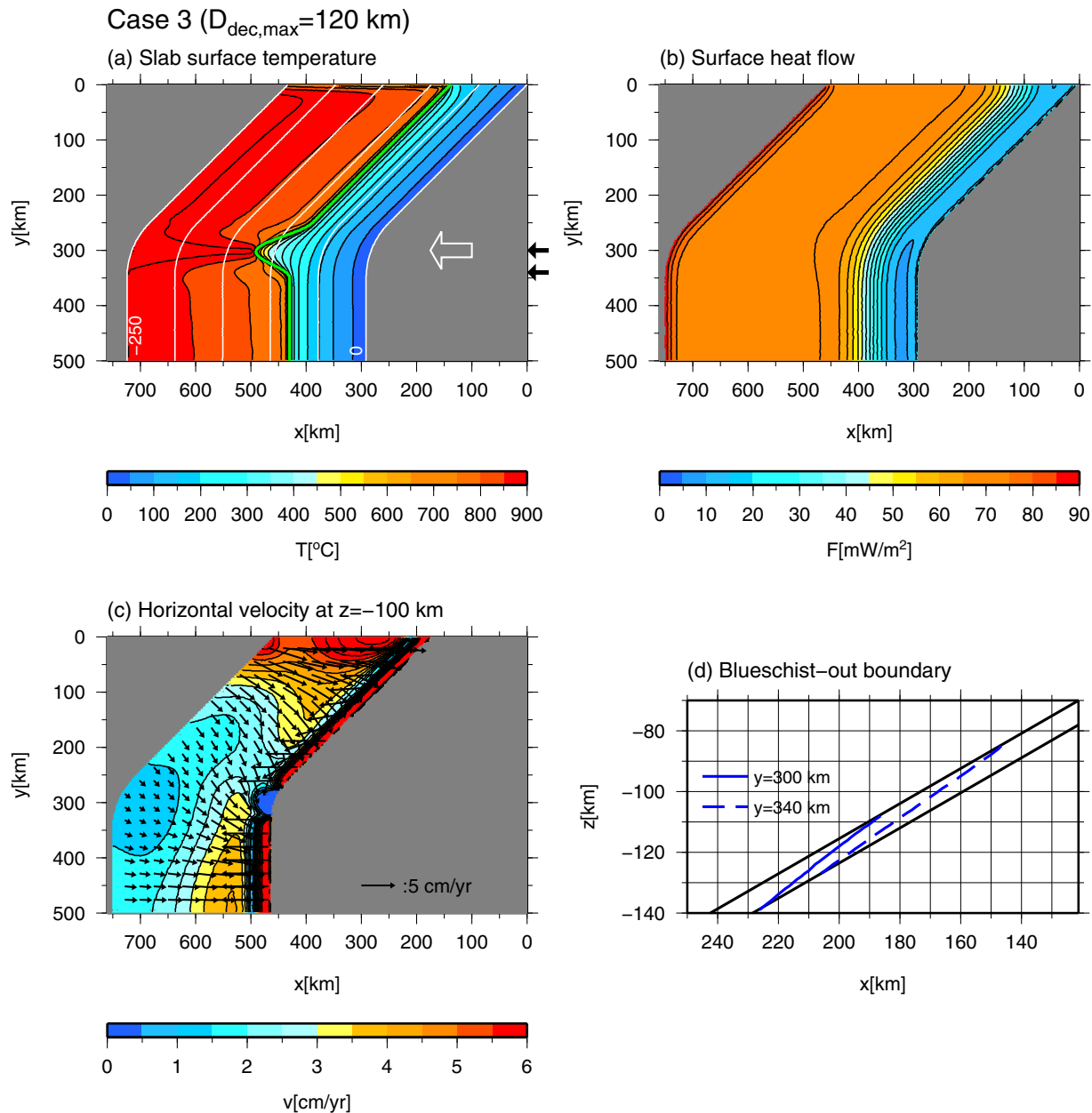
Figure A2. Results of Case 3 with the maximum slab-mantle decoupling depth ($D_{dec,max}$) extended down to 120 km with descriptions as in Figure A1.

are either warmer or cooler than expected from 2-D models. The warmer region arises through 3-D effects of thermal conduction and the colder region arises through localized slow incoming flow in the case where 3-D slab geometry is taken into account. 3-D flow arises where a local deepening of slab-mantle decoupling depth is assumed, which leads to both warmer and colder regions. The along-arc difference of slab surface temperature could reach ~100°C when large maximum slab-mantle decoupling depth (120 km) is assumed or diffusion creep is considered as the deformation mechanism. Generally, the temperature differences along the strike of the trench are modest but may be detectable by geochemical methods that determine independently the temperature of the slab below the arc. Neither the anomalous deepening of the upper plane seismicity nor the heat flow excursion in southern Hokkaido is explained well by these 3-D models, suggesting a bigger importance of structural variations in the overriding plate compounded potentially by 3-D dynamical effects that are not taken into account in this study.

Appendix A: Effects of Rheology and the Maximum Slab-Mantle Decoupling Depth

We show in this section how the results presented in this paper depends on assumed input parameters. There may be little uncertainty in 3-D slab geometry and slab velocity. Therefore, we investigate the effects of changing rheology and the maximum slab-mantle decoupling depth for Case 3.

Figure A1 shows the results of Case 3 where diffusion creep is considered as a deformation mechanism in the mantle wedge instead of dislocation creep. In this case, the effective viscosity in equation (3) is defined by

$$\eta = \left(\frac{1}{\eta_{\text{diff}}} + \frac{1}{\eta_{\text{max}}} \right)^{-1}, \tag{A1}$$

where the viscosity for diffusion creep is written as

$$\eta_{\text{diff}}(T) = A_{\text{diff}} \exp\left(\frac{E_{\text{diff}}}{RT} \right), \tag{A2}$$

where $A_{\text{diff}} = 1.3204 \times 10^9$ Pa · s is constant and $E_{\text{diff}} = 335$ kJ/mol is activation energy. The values of these parameters are based on *Karato and Wu* [1993] for dry olivine.

Slab surface temperature shows a larger variation compared to the original Case 3 (Figure A1a). It is probably because that the length scale of 3-D flow near y ∼ 300 km becomes larger (note that the general effects of using non-Newtonian viscosity is to localize the deformation in both time and space [*Christensen*, 1983, 1984]). The along-arc variation in surface heat flow is insignificant (Figure A1b). The magnitude of the flow in the mantle wedge increases as a whole (Figure A1c). Predicted blueschist-out boundaries are almost the same as those in the original Case 3 (Figure A1d).

Figure A2 shows the results of Case 3 where the maximum slab-mantle decoupling depth is extended to 120 km from 95 km. We can see that the slab surface temperature at y ∼ 300 km becomes larger than that in the original Case 3 (Figure A2a). It is because the material passes through much deeper and hence warmer part due to the assumed larger maximum slab-mantle decoupling depth. Surface heat flow does not show a large along-arc variation neither in this case (Figure A2b). The velocity field shows almost the same as the original Case 3 except for the region near y ∼ 300 km (Figure A2c). Predicted blueschist-out boundary at y = 300 km shows a large degree of deepening but still diverges from slab surface with depth, which cannot fully explain the seismicity below southern Hokkaido (Figure A2d). We also note that the depth where the blueschist-out boundary starts (∼108 km) is shallower than the assumed slab-mantle decoupling depth (120 km) in this cross section.

References

Bengtson, A. K., and P. E. van Keken (2012), Three-dimensional thermal structure of subduction zones: Effects of obliquity and curvature, *Solid Earth*, *3*, 365–373, doi:10.5194/se-3-365-2012.

Bostock, M., R. Hyndman, S. Rondenay, and S. Peacock (2002), An inverted continental Moho and serpentinization of the forearc mantle, *Nature*, *417*, 536–538.

Christensen, U. (1983), Convection in a variable-viscosity fluid: Newtonian versus power-law rheology, *Earth Planet. Sci. Lett.*, *64*, 153–162.

Christensen, U. (1984), Convection with pressure- and temperature-dependent non-Newtonian rheology, *Geophys. J. R. Astron. Soc.*, *77*, 343–384.

Conder, J. (2005), A case for hot slab surface temperatures in numerical viscous flow models in subduction zones with an improved fault zone parameterization, *Phys. Earth Planet. Inter.*, *149*, 155–164.

Cooper, L., D. Ruscitto, T. Plank, P. Wallace, E. Syracuse, and C. Manning (2012), Global variations in H$_2$O/Ce: 1. Slab surface temperatures beneath volcanic arcs, *Geochem. Geophys. Geosyst.*, *13*, Q03024, doi:10.1029/2011GC003902.

Cuvelier, C., A. Segal, and A. A. van Steenhoven (1986), Finite Element Methods and Navier-Stokes Equations, D. Reidel, Dordrecht.

Eberhart-Phillips, D., M. Reyners, M. Chadwick, and G. Stuart (2008), Three-dimensional attenuation structure of the Hikurangi subduction zone in the central North Island, New Zealand, *Geophys. J. Int.*, *174*, 418–434.

Fukao, Y., S. Widiyantoro, and M. Obayashi (2001), Stagnant slab in the upper and lower mantle transition region, *Rev. Geophys.*, *39*, 291–323.

Hacker, B. R. (2008), H$_2$O subduction beyond arcs, *Geochem. Geophys. Geosyst.*, *9*, Q03001, doi:10.1029/2007GC001707.

Hall, P. S. (2012), On the thermal evolution of the mantle wedge at subduction zones, *Phys. Earth Planet. Inter.*, *198–199*, 9–27, doi:10.1016/j.pepi.2012.03.004.

Hasegawa, A., J. Nakajima, S. Kita, T. Okada, T. Matsuzawa, and S. Kirby (2007), Anomalous deepening of a belt of intraslab earthquakes in the Pacific slab crust under Kanto, central Japan: Possible anomalous thermal shielding, dehydration reactions, and seismicity caused by shallower cold slab material, *Geophys. Res. Lett.*, *34*, L09305, doi:10.1029/2007GL029616.

Hayes, G. P., D. J. Wald, and R. L. Johnson (2012), Slab1.0: A three-dimensional model of global subduction zone geometries, *J. Geophys. Res.*, *117*, B01302, doi:10.1029/2011JB008524.

Honda, S. (1985), Thermal structure beneath Tohoku, Northeast Japan: A case study for understanding the detailed thermal structure of the subduction zone, *Tectonophysics*, *112*, 69–102.

Honda, S., and T. Yoshida (2005), Effects of oblique subduction on the 3-D pattern of small-scale convection within the mantle wedge, *Geophys. Res. Lett.*, *32*, L13307, doi:10.1029/2005GL023106.

Hyndman, R., and S. Peacock (2003), Serpentinization of the forearc mantle, *Earth Planet. Sci. Lett.*, *212*, 417–432.

Jacques, G., K. Hoernle, J. Gill, F. Hauff, H. Wehrmann, D. Garbe-Schonberg, P. van den Bogaard, I. Bindeman, and L. Lara (2013), Across-arc geochemical variations in the Southern Volcanic Zone, Chile (34.5–38.0 degrees S): Constraints on mantle wedge and slab compositions, *Geochem. Cosmochim. Acta*, *123*, 218–243.

Karato, S., and P. Wu (1993), Rheology of the upper mantle: A synthesis, *Science*, *260*, 771–778.

Katsumata, A. (2010), Depth of the Moho discontinuity beneath the Japanese islands estimated by traveltime analysis, *J. Geophys. Res.*, *115*, B04303, doi:10.1029/2008JB005864.

Kelemen, P., J. Rilling, E. Parmentier, L. Mehl, and B. Hacker (2003), Thermal structure due to solid-state flow in the mantle wedge beneath arcs, in Inside the Subduction Factory, Geophys. Monogr., vol. 138, edited by J. Eiler, pp. 293–311, AGU, Washington, D. C.

Kimura, G. (1986), Oblique subduction and collision: Forearc tectonics of the Kuril arc, *Geology*, *14*, 404–407.

Kirby, S. H., W. B. Durham, and L. A. Stern (1991), Mantle phase changes and deep-earthquake faulting in subducting lithosphere, *Science*, *252*, 216–225.

Kita, S., T. Okada, A. Hasegawa, J. Nakajima, and T. Matsuzawa (2010), Anomalous deepening of a seismic belt in the upper-plane of the double seismic zone in the Pacific slab beneath the Hokkaido corner: Possible evidence for thermal shielding caused by subducted forearc crust materials, *Earth Planet. Sci. Lett.*, *290*, 415–426, doi:10.1016/j.epsl.2009.12.038.

Kita, S., A. Hasegawa, J. Nakajima, T. Okada, T. Matsuzawa, and K. Katsumata (2012), High-resolution seismic velocity structure beneath the Hokkaido corner, northern Japan: Arc-arc collision and origins of the 1970 m 6.7 Hidaka and 1982 m 7.1 Urakawa-oki earthquakes, *J. Geophys. Res.*, *117*, B12301, doi:10.1029/2012JB009356.

Kneller, E. A., and P. E. van Keken (2008), Effect of three-dimensional slab geometry on deformation in the mantle wedge: Implications for shear wave anisotropy, *Geochem. Geophys. Geosyst.*, *9*, Q01003, doi:10.1029/2007GC001677.

Kneller, E. A., P. E. van Keken, I. Katayama, and S. Karato (2007), Stress, strain, and B-type olivine fabric in the fore-arc mantle: Sensitivity tests using high-resolution steady-state subduction zone models, *J. Geophys. Res.*, *112*, B04406, doi:10.1029/2006JB004544.

Miller, M. S., and B. L. N. Kennett (2006), Evolution of mantle structure beneath the northwest Pacific: Evidence from seismic tomography and paleogeographic reconstructions, *Tectonophysics*, *25*, TC4002, doi:10.1029/2005TC001909.

Morishige, M., and S. Honda (2013), Mantle flow and deformation of subducting slab at a plate junction, *Earth Planet. Sci. Lett.*, *365*, 132–142, doi:10.1016/j.epsl.2013.01.033.

Morishige, M., S. Honda., and P. J. Tackley (2010), Construction of semi-dynamic model of subduction zone with given plate kinematics in 3D sphere, *Earth Planets Space*, *62*, 665–673, doi:10.5047/eps.2010.09.002.

Nakajima, J., and A. Hasegawa (2006), Anomalous low-velocity zone and linear alignment of seismicity along it in the subducted Pacific slab beneath Kanto, Japan: Reactivation of subducted fracture zone?, *Geophys. Res. Lett.*, *33*, L16309, doi:10.1029/2006GL026773.

Nakajima, J., J. Shimizu, S. Hori, and A. Hasegawa (2006), Shear-wave splitting beneath the southwestern Kurile arc and northeastern Japan arc: A new insight into mantle return flow, *Geophys. Res. Lett.*, *33*, L05305, doi:10.1029/2005GL025053.

Peacock, S., and K. Wang (1999), Seismic consequences of warm versus cool subduction metamorphism: Examples from southwest and northeast Japan, *Science*, *286*, 937–939.

Plank, T., L. B. Cooper, and C. E. Manning (2009), Emerging geothermometers for estimating slab surface temperatures, *Nat. Geosci.*, *2*, 611–615, doi:10.1038/ngeo614.

Rondenay, S., G. Abers, and P. van Keken (2008), Seismic imaging of subduction zone metamorphism, *Geology*, *36*, 275–278.

Schurr, B., G. Asch, A. Rietbrock, R. Trumbull, and C. Haberland (2003), Complex patterns of fluid and melt transport in the central Andean subduction zone revealed by attenuation tomography, *Earth Planet. Sci. Lett.*, *125*, 105–119.

Stein, C. A., and S. Stein (1992), A model for the global variation in oceanic depth and heat flow with lithospheric age, *Nature*, *359*, 123–129.

Syracuse, E., P. van Keken, and G. Abers (2010), The global range of subduction zone thermal models, *Phys. Earth Planet. Inter.*, *83*, 73–90.

Tanaka, A., M. Yamano, Y. Yano, and M. Sasada (2004), Geothermal gradient and heat flow data in and around Japan (i): Appraisal of heat flow from geothermal gradient data, *Earth Planets Space*, *56*, 1191–1194.

Tsumura, N., S. Matsumoto, S. Horiuchi, and A. Hasegawa (2000), Three-dimensional attenuation structure beneath the northeastern Japan arc estimated from spectra of small earthquakes, *Tectonophysics*, *319*, 241–260.

Turner, S., J. Caulfield, M. Turner, P. van Keken, R. Maury, M. Sandiford, and G. Prouteau (2011), Recent contribution of sediments and fluids to the mantle's volatile budget, *Nat. Geosci.*, *5*, 50–54.

van Keken, P. E., B. Kiefer, and S. M. Peacock (2002), High-resolution models of subduction zones: Implications for mineral dehydration reactions and the transport of water into the deep mantle, *Geochem. Geophys. Geosyst.*, *3*(10), 1056, doi:10.1029/2001GC000256.

van Keken, P. E., et al. (2008), A community benchmark for subduction zone modeling, *Phys. Earth Planet. Inter.*, *171*, 187–197.

van Keken, P. E., S. Kita, and J. Nakajima (2012), Thermal structure and intermediate-depth seismicity in the Tohoku-Hokkaido subduction zones, *Solid Earth*, *3*, 355–364, doi:10.5194/se-3-355-2012.

Wada, I., and K. Wang (2009), Common depth of slab-mantle decoupling: Reconciling diversity and uniformity of subduction zones, *Geochem. Geophys. Geosyst.*, *10*, Q10009, doi:10.1029/2009GC002570.

Wada, I., K. Wang, J. He, and R. D. Hyndman (2008), Weakening of the subduction interface and its effects on surface heat flow, slab dehydration, and mantle wedge serpentinization, *J. Geophys. Res.*, *113*, B04402, doi:10.1029/2007JB005190.

Wada, I., C. Rychert, and K. Wang (2011), Sharp thermal transition in the forearc mantle wedge as a consequence of nonlinear mantle wedge flow, *Geophys. Res. Lett.*, *38*, L13308, doi:10.1029/2011GL047705.

Watt, S., D. Pyle, T. Mather, and J. Naranjo (2013), Arc magma compositions controlled by linked thermal and chemical gradients above the subducting slab, *Geophys. Res. Lett.*, *40*, 2550–2556, doi:10.1002/grl.50513.

Wessel, P., and W. H. F. Smith (1998), New improved version of the generic mapping tools released, *EOS Trans. AGU*, *79*, 579.

Zhao, D., T. Matsuzawa, and A. Hasegawa (1997), Morphology of the subducting slab boundary in the northeastern Japan arc, *Phys. Earth Planet. Inter.*, *102*, 89–104.